Biomedical Optics EXPRESS

Cross-phase modulation spectral shifting: nonlinear phase contrast in a pump-probe microscope

Jesse W. Wilson,[1] Prathyush Samineni,[1] Warren S. Warren,[1,2,3] and Martin C. Fischer[1,*]

[1]*Department of Chemistry, Duke University, Durham, North Carolina 27708, USA*
[2]*Department of Radiology, Duke University Medical Center, Durham, North Carolina 27710, USA*
[3]*Department of Biomedical Engineering, Duke University, Durham, North Carolina 27708, USA*
**martin.fischer@duke.edu*

Abstract: Microscopy with nonlinear phase contrast is achieved by a simple modification to a nonlinear pump-probe microscope. The technique measures cross-phase modulation by detecting a pump-induced spectral shift in the probe pulse. Images with nonlinear phase contrast are acquired both in transparent and absorptive media. In paraffin-embedded biopsy sections, cross-phase modulation complements the chemically-specific pump-probe images with structural context.

OCIS codes: (180.4315) Nonlinear microscopy; (190.7110) Ultrafast nonlinear optics; (170.3880) Medical and biological imaging.

References and links

1. D. Fu, T. E. Matthews, T. Ye, I. R. Piletic, and W. S. Warren, "Label-free in vivo optical imaging of microvasculature and oxygenation level," J. Biomed. Opt. **13**(4), 040503 (2008).
2. T. E. Matthews, I. R. Piletic, M. A. Selim, M. J. Simpson, and W. S. Warren, "Pump-probe imaging differentiates melanoma from melanocytic nevi," Sci. Transl. Med. **3**(71), 71ra15 (2011).
3. P. Samineni, A. deCruz, T. E. Villafaña, W. S. Warren, and M. C. Fischer, "Pump-probe imaging of historical pigments used in paintings," Opt. Lett., doc. ID 160175 (posted 29 February 2012, in press).
4. P. Mahou, N. Olivier, G. Labroille, L. Duloquin, J.-M. Sintes, N. Peyriéras, R. Legouis, D. Débarre, and E. Beaurepaire, "Third-harmonic generation, four-wave mixing microscopy of tissues and embryos," Biomed. Opt. Express **2**(10), 2837–2849 (2011).
5. K. Ekvall, P. van der Meulen, C. Dhollande, L.-E. Berg, S. Pommeret, R. Naskrecki, and J.-C. Mialocq, "Cross phase modulation artifact in liquid phase transient absorption spectroscopy," J. Appl. Phys. **87**(5), 2340 (2000).
6. C. W. Freudiger, W. Min, B. G. Saar, S. Lu, G. R. Holtom, C. He, J. C. Tsai, J. X. Kang, and X. S. Xie, "Label-free biomedical imaging with high sensitivity by stimulated Raman scattering microscopy," Science **322**(5909), 1857–1861 (2008).
7. M. C. Fischer, T. Ye, G. Yurtsever, A. Miller, M. Ciocca, W. Wagner, and W. S. Warren, "Two-photon absorption and self-phase modulation measurements with shaped femtosecond laser pulses," Opt. Lett. **30**(12), 1551–1553 (2005).
8. M. C. Fischer, H. C. Liu, I. R. Piletic, and W. S. Warren, "Simultaneous self-phase modulation and two-photon absorption measurement by a spectral homodyne Z-scan method," Opt. Express **16**(6), 4192–4205 (2008).
9. P. Samineni, Z. Perret, W. S. Warren, and M. C. Fischer, "Measurements of nonlinear refractive index in scattering media," Opt. Express **18**(12), 12727–12735 (2010).
10. P. Samineni, B. Li, J. W. Wilson, W. S. Warren, and M. C. Fischer, "Cross-phase modulation imaging," Opt. Lett. **37**(5), 800–802 (2012).
11. G. P. Agrawal, P. L. Baldeck, and R. R. Alfano, "Temporal and spectral effects of cross-phase modulation on copropagating ultrashort pulses in optical fibers," Phys. Rev. A **40**(9), 5063–5072 (1989).
12. P. Chapple, J. Staromlynska, J. Hermann, T. Mckay, and R. McDuff, "Single-beam Z-scan: measurement techniques and analysis," J. Nonlinear Opt. Phys. Mater. **6**(3), 251–294 (1997).
13. P. Tian and W. S. Warren, "Ultrafast measurement of two-photon absorption by loss modulation," Opt. Lett. **27**(18), 1634–1636 (2002).
14. N. S. Makarov, M. Drobizhev, and A. Rebane, "Two-photon absorption standards in the 550-1600 nm excitation wavelength range," Opt. Express **16**(6), 4029–4047 (2008).
15. Reference [14] defined the TPA cross section with an extra factor of two that is divided out here for direct comparison to the value in Ref. [13].
16. E. T. J. Nibbering, M. A. Franco, B. S. Prade, G. Grillon, C. Le Blanc, and A. Mysyrowicz, "Measurement of the nonlinear refractive index of transparent materials by spectral analysis after nonlinear propagation," Opt. Commun. **119**(5-6), 479–484 (1995).

#164372 - $15.00 USD Received 9 Mar 2012; revised 1 Apr 2012; accepted 3 Apr 2012; published 4 Apr 2012

17. A. Vogel, J. Noack, G. Hüttman, and G. Paltauf, "Mechanisms of femtosecond laser nanosurgery of cells and tissues," Appl. Phys. B **81**(8), 1015–1047 (2005).
18. U. K. Tirlapur, K. König, C. Peuckert, R. Krieg, and K. J. Halbhuber, "Femtosecond near-infrared laser pulses elicit generation of reactive oxygen species in mammalian cells leading to apoptosis-like death," Exp. Cell Res. **263**(1), 88–97 (2001).
19. K. König, P. T. C. So, W. W. Mantulin, and E. Gratton, "Cellular response to near-infrared femtosecond laser pulses in two-photon microscopes," Opt. Lett. **22**(2), 135–136 (1997).
20. I. R. Piletic, T. E. Matthews, and W. S. Warren, "Probing near-infrared photorelaxation pathways in eumelanins and pheomelanins," J. Phys. Chem. A **114**(43), 11483–11491 (2010).
21. R. Lazova and J. M. Pawelek, "Why do melanomas get so dark?" Exp. Dermatol. **18**(11), 934–938 (2009).
22. D. Débarre and E. Beaurepaire, "Quantitative characterization of biological liquids for third-harmonic generation microscopy," Biophys. J. **92**(2), 603–612 (2007).
23. M. C. Fischer, H. C. Liu, I. R. Piletic, Y. Escobedo-Lozoya, R. Yasuda, and W. S. Warren, "Self-phase modulation signatures of neuronal activity," Opt. Lett. **33**(3), 219–221 (2008).
24. H. S. Sakhalkar, M. Dewhirst, T. Oliver, Y. Cao, and M. Oldham, "Functional imaging in bulk tissue specimens using optical emission tomography: fluorescence preservation during optical clearing," Phys. Med. Biol. **52**(8), 2035–2054 (2007).
25. A. Gnoli, L. Razzari, and M. Righini, "Z-scan measurements using high repetition rate lasers: how to manage thermal effects," Opt. Express **13**(20), 7976–7981 (2005).

1. Introduction

Nonlinear pump-probe microscopy enables label-free, chemically specific imaging of absorptive pigments such as oxy- and deoxy-hemoglobin in microvasculature [1], eumelanin and pheomelanin in pigmented lesions such as melanomas [2,3], and even historical pigments in artwork [3]. The interpretation of a pump-probe image may be enhanced by structural context from a complementary imaging modality. Recently, complementary information from four wave mixing (4WM) has been shown to resolve ambiguities in interpreting third harmonic generation (THG) images [4]. In pump-probe interactions, the same nonlinear optical property that enables 4WM—the real part of the third-order optical susceptibility $\chi^{(3)}$—gives rise to cross-phase modulation (XPM). XPM is sometimes viewed as an artifact in

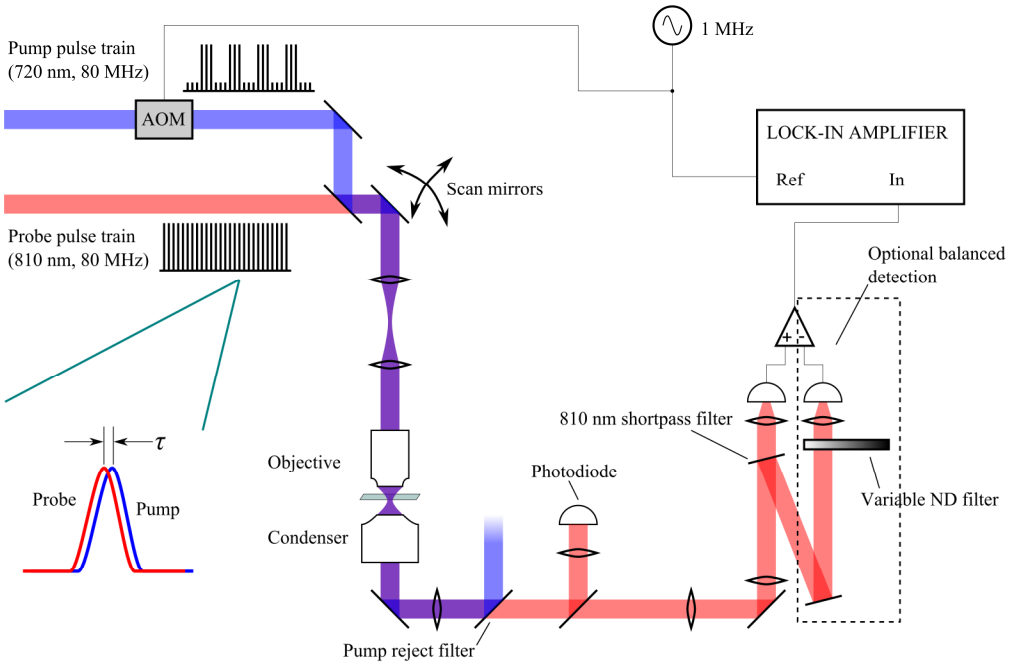

Fig. 1. The optical set-up for XPMSS imaging involves adding a shortpass filter to an existing pump-probe microscope. Optionally a balanced photodiode can be used to isolate nonlinear phase modulation from nonlinear absorption.

#164372 - $15.00 USD Received 9 Mar 2012; revised 1 Apr 2012; accepted 3 Apr 2012; published 4 Apr 2012

pump-probe spectroscopy [5] (which can be suppressed by using a high numerical aperture condenser [6]). Here we demonstrate that simple modifications to a pump-probe microscope enable a new technique, cross-phase modulation spectral shifting (XPMSS), which can complement pump-probe microscopy with structural information even in situations where linear techniques (i.e. linear transmittance and confocal reflectance) are obscured by scattering.

XPMSS is closely related to other methods that encode measurements of the third-order optical susceptibility $\chi^{(3)}$ in the spectral domain using femtosecond pulse shaping [7,8]. These methods are robust in scattering media [9], and have been applied to image biological specimens [10]. The XPMSS technique presented here does not require a pulse shaper, is quickly interchangeable with a pump-probe imaging set-up, and is able to acquire images with high signal-to-noise ratio (SNR), using optical intensities suitable for tissue imaging. Robustness against linear and nonlinear absorption artifacts is achieved by detecting the spectral shifting with a balanced photodiode and linear projection of acquired data onto a reference XPMSS probe delay scan. Our imaging results show that XPMSS provides high structural contrast both in transparent biological specimens and in highly absorptive specimens embedded in scattering media.

2. Setup and theory

The experimental arrangement employs a standard pump-probe configuration, shown in Fig. 1, where the pump is modulated at 1 MHz with an acousto-optic modulator (AOM), and a motorized delay stage controls pump-probe delay, τ. Probe and pump pulses are supplied by a Ti:sapph oscillator (Spectra-Physics Tsunami), and an intracavity-doubled optical parametric oscillator (Coherent Mira OPO), capable of providing pump and probe wavelength combinations from 520 nm down to 880 nm. The pump and probe pulses are focused onto a sample with a microscope objective (here we use either a 10x / 0.25 NA dry or a 40x / 0.8 NA water immersion) and re-collimated afterwards by 1.1 NA condenser (the high-NA condenser helps to minimize artifacts from thermal lensing and Kerr lensing [6]).

Cross-phase modulation (XPM) shifts the probe pulse spectrum in a manner that depends on the pump-probe delay τ [11]. This shift may be detected by splitting the probe pulse at its center wavelength, and looking for an imbalance between the two spectral halves. After the condenser, the pump is rejected and the probe beam is split at its center wavelength by a dielectric filter (Chroma D800/20m), angle-tuned to set the filter cutoff at the center of the probe spectrum. The transmitted half of the probe spectrum is directed onto a photodiode. Any shift $\Delta\omega$ in the probe spectrum caused by XPM interaction with the modulated pump results in 1 MHz modulation of the probe intensity transmitted through the filter; this signal is detected with a lock-in amplifier. Optionally, a high-speed balanced photodiode (NewFocus model 2307) may be used to suppress other nonlinear pump-probe interactions that do not shift the probe spectrum (such as nonlinear absorption).

As the probe pulse propagates through the sample, it accumulates phase from both the linear and nonlinear indexes of refraction:

$$\varphi(t) = \left[n_0 + n_{2,\mathrm{SPM}} I_{\mathrm{pr}}(t) + n_{2,\mathrm{XPM}} I_{\mathrm{pu}}(t) \right] \frac{\omega_{\mathrm{pr}} L}{c}. \qquad (1)$$

Here, n_0 is the linear index of refraction, $n_{2,\mathrm{SPM}} \propto Re\{\chi^{(3)}(-\omega_{\mathrm{pr}}; \omega_{\mathrm{pr}}, \omega_{\mathrm{pr}}, -\omega_{\mathrm{pr}})\}$ is the nonlinear index mediating self-phase modulation, $n_{2,\mathrm{XPM}} \propto Re\{\chi^{(3)}(-\omega_{\mathrm{pr}}; \omega_{\mathrm{pr}}, \omega_{\mathrm{pu}}, -\omega_{\mathrm{pu}})\}$ is the nonlinear index mediating cross-phase modulation, $I_{\{\mathrm{pu,pr}\}}(t)$ are the pump and probe pulse temporal intensity profiles, $\omega_{\{\mathrm{pu,pr}\}}$ are the pump and probe angular frequencies, L is the effective interaction length, and c is the velocity of light in vacuum. The pump-induced XPM term, $n_{2,\mathrm{XPM}} I_{\mathrm{pu}}(t)$, may be isolated from the other terms by modulating the pump with an AOM, then filtering the photodiode's output with a lock-in amplifier.

To roughly estimate the expected signal amplitude, consider a pump-probe delay τ such that the peak of the probe pulse coincides with the steepest slope of the pump pulse (on either

#164372 - $15.00 USD Received 9 Mar 2012; revised 1 Apr 2012; accepted 3 Apr 2012; published 4 Apr 2012

the rising or the falling half of the pump pulse). The resulting XPM may be approximately regarded as linear across the probe pulse in time; this linear temporal phase produces a spectral shift in the probe:

$$\Delta\omega = -\frac{d\varphi}{dt} = -\frac{\omega_{\mathrm{pr}}}{c} L n_{2,\mathrm{XPM}} \left(\frac{dI_{\mathrm{pu}}}{dt} \right)_{t=\tau}. \quad (2)$$

The change in detected intensity (on a single photodiode) in a spectrally shifted probe is

$$\Delta S = \int_{-\infty}^{\omega_0} I_{\mathrm{pr}}(\omega)\, d\omega - \int_{-\infty}^{\omega_0} I_{\mathrm{pr}}(\omega - \Delta\omega)\, d\omega = \int_{0}^{\Delta\omega} I_{\mathrm{pr}}(\omega)\, d\omega = I_0 \mathrm{erf}\left(\frac{t_{\mathrm{fwhm}}\, \Delta\omega}{2\sqrt{\ln 2}} \right). \quad (3)$$

For a balanced detector, the intensity incident on one photodiode increases by ΔS, while the intensity incident on the other photodiode decreases by ΔS; the total signal in this case is $2\Delta S$.

Consider the case where both pump and probe pulses have Gaussian intensity profiles with full-width at half maximum duration t_{fwhm}. Centering the probe on the rising slope of the pump shifts the probe to higher frequency; centering the probe on the falling slope of the pump shifts the probe to lower frequency. The maximum spectral shift will be imparted at $\tau = t_{\mathrm{fwhm}} / \sqrt{8 \ln 2}$, where

$$\left(\frac{dI_{\mathrm{pu}}}{dt} \right)_{\mathrm{max}} = I_0 \sqrt{\frac{8 \ln 2}{e}} \frac{1}{t_{\mathrm{fwhm}}}. \quad (4)$$

Of course, this shift applied to only a small portion of the pulse. A more precise numerical calculation is straightforward with the exact pulse shape, as discussed later, but other factors affect the measurement (such as beam spatial mode quality, residual uncompensated dispersion, and spatial overlap) [12] so this is only an estimate.

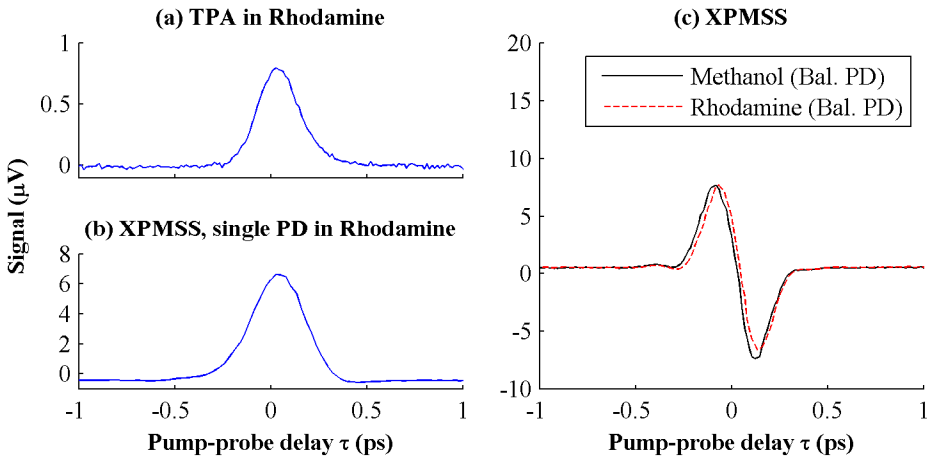

Fig. 2. (a) Pump-probe delay scan of 5 mM R6G in methanol, single photodiode without the probe shortpass edge filter. (b) Scan of 30 mM R6G in methanol, single photodiode with the probe shortpass edge filter. (c) XPMSS delay scans of methanol and 30 mM R6G dissolved in methanol with balanced photodiode. Though R6G has a large nonlinear absorption cross section, the balanced photodiode robustly measures XPM spectral shift, rejecting amplitude modulation

#164372 - $15.00 USD Received 9 Mar 2012; revised 1 Apr 2012; accepted 3 Apr 2012; published 4 Apr 2012

3. Results

3.1 Pump-probe spectroscopy / transient response

To demonstrate the spectral shifting based XPM measurement technique and to show that a balanced photodiode effectively subtracts nonlinear absorption we performed pump-probe delay scans of rhodamine-6G (R6G), chosen for its strong nonlinear absorption cross-section (15 GM at 800 nm, 27.5 GM at 750 nm, and 5 GM at 650 nm [13–15]). We compare pure methanol and a 30 mM solution of R6G in methanol using a simplified optical set-up outside the microscope, in which the combined beams are directly focused into a cuvette of 1 mm path length by a 10x 0.25 NA objective (back aperture underfilled by 30%, NA_{eff} = 0.075). The pump and probe pulses used in these measurements were both of approximately 175 fs duration (estimated from the cross-correlation shown in Fig. 2(a)): pump wavelength of 672 nm with 16 mW average power; probe wavelength of 794 nm with 18 mW average power.

The resulting data in Fig. 2 show pump-probe delay scans for several different conditions. Figure 2(a) shows a standard pump-probe delay scan of 5 mM R6G with a single photodiode and only the pump rejection filter (no shortpass filter) before the photodiode. With the selected pump-probe wavelengths, this reflects sum-frequency absorption when the pulses are overlapped; the resulting delay scan is essentially a cross-correlation of the pump and probe pulses. In Fig. 2(b), the experiment is repeated with 30 mM R6G and the addition of a 792 nm shortpass filter to split the probe spectrum in front of the single photodiode; at this concentration, the nonlinear absorption in the dye completely overwhelms any XPMSS signal. However, Fig. 2(c) demonstrates this nonlinear absorption is cancelled when a balanced photodiode is employed. The XPMSS pump-probe delay scans exhibit a characteristic dispersive shape, since alignment of the probe with the rising or falling slopes of the pump pulse shifts the spectrum in opposite directions. Each delay scan took less than a minute to acquire, and has a signal to noise ratio of ~250 (calculated as the peak value divided by the standard deviation of the signal for $\tau > 0.5$ ps, where there is no pump-probe overlap).

To compare the experimental results in Fig. 2(c) with theory, a back-of the envelope estimate of the XPMSS signal follows. The pump pulse peak intensity under these focal conditions is I_0 = 77 GW/cm^2. The maximum slope of the pump pulse is 5.3 TW·cm^{-2}·ps^{-1}. The nonlinear refractive index of methanol is $n_2 \approx 3 \times 10^{-16}$ cm^2/W [16]. The signal on the balanced photodiode for half of the spectrum is 0.64 V (taking into consideration the Si detector sensitivity of 0.5 A/W at 800 nm, 1.4 V/mA amplifier gain at 1 MHz, and an ND filter with 1.0 OD in front of the detector). We numerically compute the spectral shift the probe by applying a Gaussian phase, offset in time by τ, resulting in an expected shift of 3.7×10^{-4} nm, which will yield a lock-in signal amplitude of 28 μV_{RMS}. As mentioned above, this is an upper limit on the XPMSS signal; factors such as imperfect spatial overlap reduce the signal observed in experiment.

3.2 Live cell imaging with cross-phase modulation

In Fig. 3 we image a single layer of epidermal cells from an onion with pump and probe wavelengths of 720 nm and 810 nm, respectively. An image stack is acquired as a function of varying pump-probe delay τ to confirm that the spectrally filtered probe signal has the same dispersive profile expected of an XPMSS measurement. Figure 3(a) shows a single image acquired at τ = 100 fs, found to give the maximum spectral shift. To show the XPMSS dispersive time delay profile, two regions of interest are highlighted; the averaged delay scans for each region is shown in Fig. 3(b), in good agreement with what we expect from Fig. 2(c). The contrast available with XPMSS can be doubled by subtracting the signal at the negative XPMSS peak (t = −100fs) from the signal at the positive XPMSS peak (t = −100 fs); this XPMSS difference image is shown in Fig. 3(c). For comparison, the linear transmissivity image is shown in Fig. 3(d).

#164372 - $15.00 USD Received 9 Mar 2012; revised 1 Apr 2012; accepted 3 Apr 2012; published 4 Apr 2012

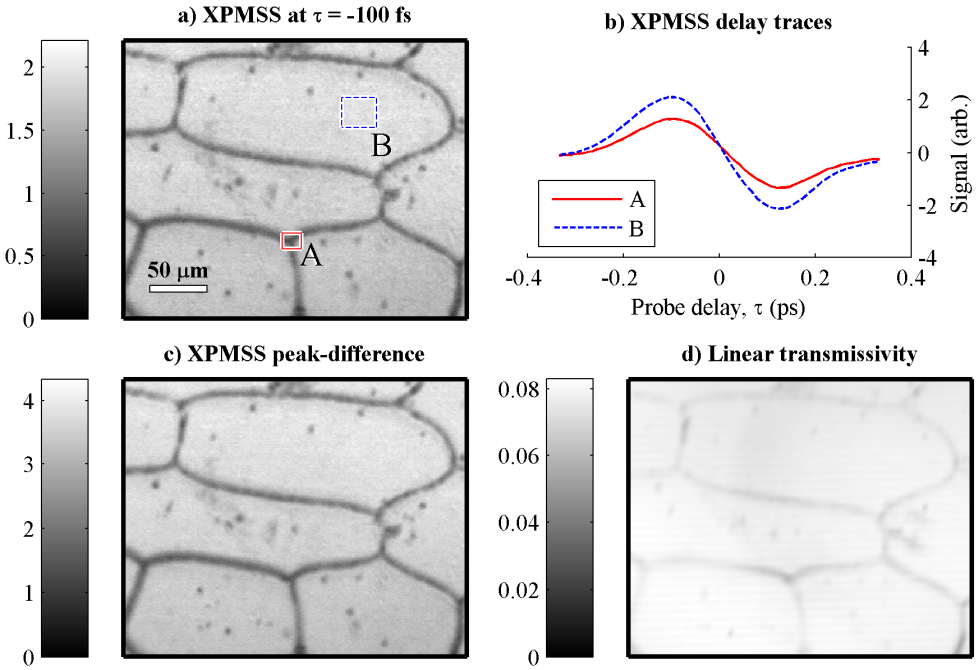

Fig. 3. XPM spectral shifting in a fresh onion epidermis with a 10x 0.25 NA objective. (a) Image at a single delay, −100 fs. (b) Delay scans for regions of interest in cytoplasm (blue curve) and cell wall (red curve); both exhibit spectral shifting characteristic of cross-phase modulation. (c) contrast enhanced by subtracting the images taken at the two delays with peak XPM spectral shifting response (at −100 fs and + 100 fs). (d) transmissivity image for comparison. Appx. 7 seconds per frame, 83 mW total power incident at sample.

The total optical power employed here was 83 mW—enough to warrant consideration of damage to the cells under study. In this regime (~100 fs duration, 80 MHz pulses of near-infrared wavelength), the primary concern is from accumulation of chemical damage triggered by laser-induced low-density plasma formation [17]. The intensity at which the free electron density reaches an average of one free electron per focal volume is as low as 0.26 TW/cm^2 [17], and cell death through apoptosis has been demonstrated with as little as 0.44 TW/cm^2 [18]. For the images in Fig. 3, the peak intensity is lower than both these numbers: 83 mW through a 0.25 NA, underfilled by 72% (NA_{eff} = 0.18) objective, is 0.18 TW/cm^2, comparable to the safe intensity level of 0.12 TW/cm^2 reported in Ref [19].

3.3 Melanoma biopsy imaging

To see if XPMSS is capable of providing structural contrast in situations where linear reflectance and transmission are obscured by scattering, we examine a pigmented cell in a 5 μm-thick unstained skin biopsy section, embedded in paraffin wax. As shown in Fig. 4(a) and 4(b), the scattering from the wax obscures cellular detail in both the linear transmissivity and reflectance confocal images. Using nonlinear pump-probe microscopy and principal

#164372 - $15.00 USD Received 9 Mar 2012; revised 1 Apr 2012; accepted 3 Apr 2012; published 4 Apr 2012

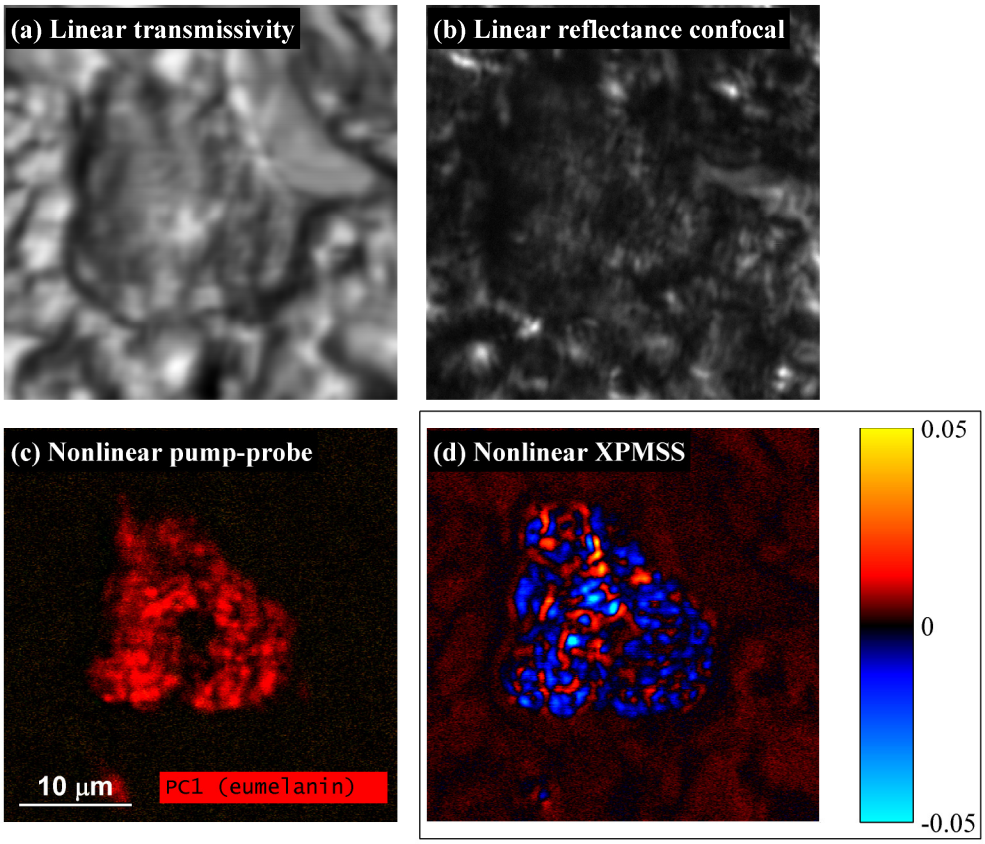

Fig. 4. Pigmented cell imaging. (a) Linear transmissivity image, obscured by scattering in the embedding paraffin wax. (b) Linear reflectance confocal image. (c) Pump-probe principal component image [2]. (d) Extracted XPMSS, using balanced photodiode. Images acquired with a 40x 0.8 NA water immersion objective, with 710 nm pump at 3.8 mW, 810 nm probe at 3.8 mW incident on the sample. Dwell time 48 μs/pixel; appx. 12 sec. per frame; 26 pump-probe delays acquired. Power reduced to 1.1 mW each for (c) to avoid saturating detection electronics.

component analysis [2], the cell's pigmentation chemistry content is imaged, as shown in Fig. 4(c), and determined to be primarily composed of eumelanin (the pump-probe image is acquired with lower intensity than the XPMSS images; dense melanin is highly absorptive, producing a signal that saturates our detection electronics in pump-probe configuration with the power levels used to detect XPMSS). To provide structural contrast, an XPMSS delay stack is acquired with a balanced photodiode as described above, with peak intensity comparable to that used in Fig. 3 (7.6 mW through $NA_{eff} = 0.57$ corresponds to 0.17 TW/cm^2). Pixels outside the cell exhibited the characteristic dispersive XPMSS delay scan shown in Fig. 2(c) and Fig. 3(b), while pixels with heavy eumelanin content exhibited a delay scan which appeared to be a superposition of XPMSS, transient absorption (TA) from eumelanin, and a long-lived thermal offset [2,20]. The thermal offset is removed by subtracting from each pixel the signal at a negative delay, for which there is no pump-probe overlap and the probe passes through the sample before the pump can promote electrons to the excited state. The presence of residual TA signal might be related to the wavelength-dependent nature of melanin's excited state dynamics [20], causing an imbalance on the balanced detector. The XPMSS and TA signals may be roughly distinguished as follows: for $\tau < 0$, XPMSS is positive, while eumelanin transient absorption exhibits little signal; for $\tau > 0$, XPMSS is negative, while eumelanin transient absorption is positive. To generate an image isolating the

#164372 - $15.00 USD Received 9 Mar 2012; revised 1 Apr 2012; accepted 3 Apr 2012; published 4 Apr 2012

two components, we calculate the dot product of each pixel's delay scan against a characteristic XPMSS delay scan (which is selected from pixels outside the pigmented cell). Positive dot product values indicate an XPMSS signal, while negative values indicate residual transient absorption. The resulting dot product image is shown in Fig. 4(d). The XPMSS dot product image reveals details that are complementary to the pump-probe image. Outside the cell, dermal collagen is visible; inside the cell, XPMSS reveals subcellular structure that is obscured by scattering in both the linear transmissivity and confocal images. Such subcellular structures may assist identifying whether a pigmented cell is a melanocyte or macrophage, an important distinction in diagnosing melanoma [21].

In situations where pigmentation is less dense, the dot product analysis alone may be sufficient to separate XPMSS from transient absorption without the need for a balanced detector. To demonstrate this, we imaged a wider field of view of the dermo-epidermal junction in an unstained biopsy section of a melanoma using a normal photodiode. The pump-probe image is shown in Fig. 5(a), and for comparison with other commonly employed nonlinear methods for dermatological imaging, Fig. 5(b) shows an image of second harmonic generation (SHG) and multiphoton autofluorescence (both acquired episcopically with a single PMT behind a 680 nm dichroic and a BG40 glass filter). Figure 5(c) shows the XPMSS dot product image, generated with the same technique used for Fig. 4(d). As with the image of the single pigmented cell, the pump-probe image here shows uniform eumelanin content. This pigment-specific image is complemented by structural details in both the autofluorescence/SHG and XPMSS images. The SHG signal originates in the dermal collagen, and is an order of magnitude more intense than the epidermal autofluorescence signal. In the XPMSS image, fine details are observed in the dermal collagen, and outlines of cell nuclei can be discerned. Here, the XPMSS dot product clearly separates XPMSS from the excited state absorption response of eumelanin, even without balanced detection.

4. Conclusions

We have shown that a modified pump-probe detection scheme can produce nonlinear cross-phase modulation images that complement the pump-probe images of pigment. Residual absorptive signal is removed by using a balanced photodiode or by projecting the delay scan onto a reference signal. In transparent samples, XPMSS appears similar to linear transmissivity, but with higher contrast. In specimens where scattering obscures linear contrast, XPMSS produces clear contrast. The XPMSS technique is essentially a homodyne 4-wave mixing (4WM) microscopy, achieved by simply adding an optical filter to the detectionarm of a pump-probe microscope. While previous reports of 4WM microscopy require sensitive photon counting detection [4], XPMSS can be imaged with an ordinary photodiode and low optical intensities. Though we employed a balanced photodiode and separate pump–probe wavelengths, XPMSS may also be detected in a simpler arrangement. Any pump-probe microscope can be adapted by the addition of a short-pass filter in front of a single (not balanced) detector. To ensure separation of XPMSS from transient absorption (TA), the dot product method works well, provided the two signals have opposite sign, as with the eumelanin demonstration here. In principle, a long-pass filter could be used instead to reverse the sign of the XPMSS signal for greater flexibility. Furthermore, the complexity of a two-color source can be replaced with a degenerate pump-probe wavelengths, provided the pump pulse is rejected before detection (either spatially, using a crossed-beam geometry in the sample, or by using orthogonal pump-probe polarizations).

In addition to providing complementary structural contrast in pump-probe imaging, there are numerous potential applications of XPMSS both for imaging and nonlinear spectroscopy. First, the high sensitivity of XPMSS may be able to sense changes in ion concentration. Studies with third harmonic generation (THG) have confirmed that $\chi^{(3)}$ depends on ion concentration, though THG images are more sensitive to cell geometry than to actual ion concentration [22]. However, 4WM and XPM are sensitive to the third-order susceptibility itself, and may provide a more direct measurement of ion concentration. This application may lead to label-free optical imaging of neuronal activity [23]. Second, XPMSS may be useful for

#164372 - $15.00 USD Received 9 Mar 2012; revised 1 Apr 2012; accepted 3 Apr 2012; published 4 Apr 2012

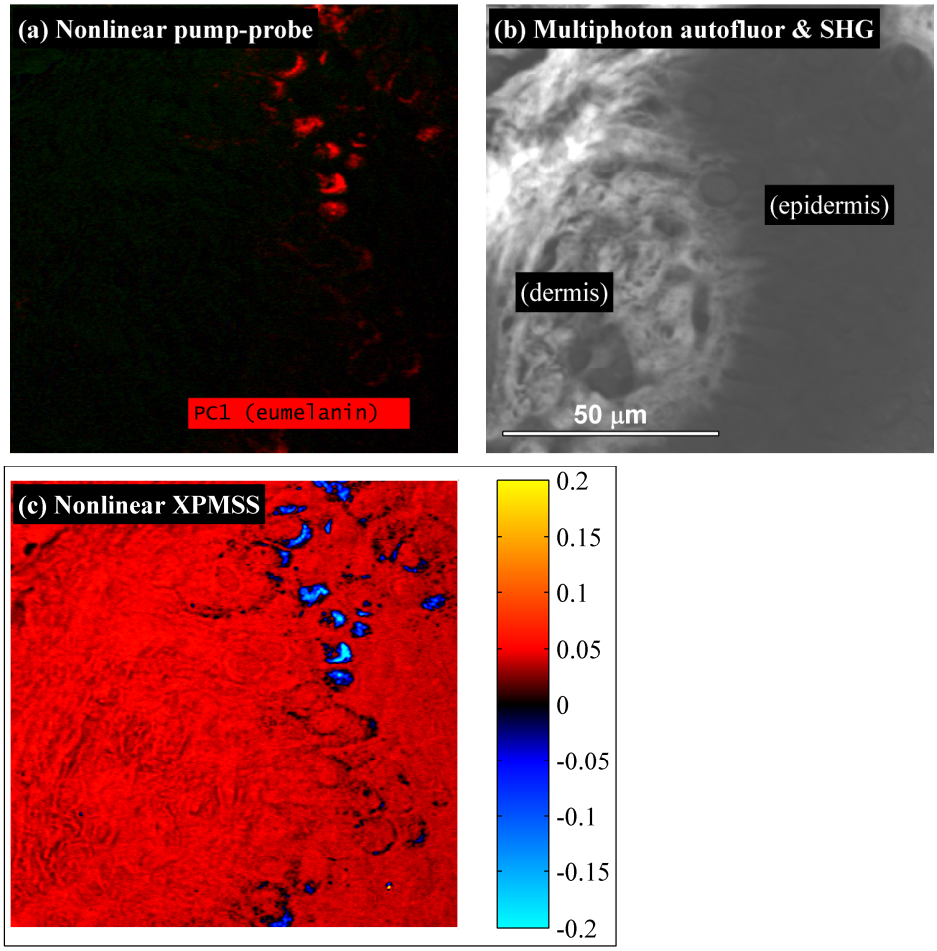

Fig. 5. Images of the dermo-epidermal junction in a melanoma biopsy. a) Pump-probe image showing uniform eumelanin content. b) Combined multiphoton autofluorescence and SHG (imaged with a single PMT). c) XPMSS dot product image. Images acquired with a 40x 0.8 NA water immersion objective, 5 mW 720 nm pump, 5 mW 810 nm probe, 49 delays, 4 frame averaging.

imaging optically cleared specimens. Most fluorescent labels bleach with repetitive imaging. Special care must be taken to preserve fluorescence in the process of specimen preservation and optical clearing. The fluorophores that survive the clearing process are only good for a limited amount of imaging, as the excitation light causes photobleaching [24]. In pump-probe spectroscopy, XPMSS characterization could help clean up unwanted coherent artifacts near time-zero [5]. In z-scan measurements with high repetition rate lasers, which rely on sensing changes in spatial mode, it is challenging to separate the desired n_2 Kerr lensing from thermal lensing [25]; in the XPMSS method, because thermal diffusion timescales are orders of magnitude longer than the < 1 picosecond timescale of the temporal phase modulation, thermal effects are readily separable. Finally, XPMSS could also be used to measure off-diagonal tensor elements of the third-order susceptibility $\chi^{(3)}$ by rotating the polarization of the pump and probe pulses.

Acknowledgments

This study was funded by the Duke University and the NIH (grant no. 1RC1CA145105).

#164372 - $15.00 USD Received 9 Mar 2012; revised 1 Apr 2012; accepted 3 Apr 2012; published 4 Apr 2012